Table 2
Univariate Cox regression analysis of survival relative to *SREBF1* protein expression and clinicopathological parameters.

Variables (*n*)	HR (95% CI)	*P*-value
SREBF1 and mortality ($n = 54$)		
Tumor size		
<3 cm ($n = 37$)	1	
⩾3 cm ($n = 17$)	2.2 (0.6–8.3)	0.2
pTNM stage		
I, II ($n = 45$)	1	
III, IV ($n = 9$)	2.0 (0.4–9.4)	0.4
Serum AFP		
<20 ng/ml ($n = 35$)	1	
⩾20 ng/ml (n = 19)	1.5 (0.4–5.4)	0.5
SREBF1		
Low ($n = 34$)	1	
High ($n = 20$)	3.7 (1.0–13.7)	0.05

Because the majority of our HCC patients analyzed had Child–Pugh class A scores and about 70% had tumors less than 3 cm in diameter, all were expected to have a good prognosis. Indeed, patient survival in this cohort was not segregated by tumor size or pTNM stage (Table 2). Although the sample size was relatively small, we found that enhanced expression of *SREBF1* was a prognostic factor for mortality in HCC possibly due to the highly proliferative nature. Activation of lipogenesis pathways, as shown by overexpression of *FASN*, has been found to correlate with high mortality in breast, prostate, and lung cancer [43], suggesting that activation of lipogenesis may be a fundamental characteristic of cancer with poor prognosis. Thus, *SREBF1* expression may be a good biomarker for HCC classification, a finding that should be validated in a large scale cohort. Because deactivation of the lipogenesis pathway by inhibition of *SREBF1* gene expression could inhibit HCC cell growth *in vitro*, *SREBF1* may be a good target for pharmaceutical intervention in these tumors.

In conclusion, our genome-wide gene expression profiling analyses found that the lipogenesis pathway was activated in a subset of HCC. *SREBF1*, which activates the lipogenesis pathway, may be a good biomarker for HCC prognosis and may be a good target for therapeutic intervention.

Acknowledgements

We are grateful to the members of The Liver Disease Center at Kanazawa University Hospital for providing data of human liver tissue samples. We would also like to thank Dr. Hitoshi Shimano for providing invaluable reagents.

Appendix A. Supplementary data

Supplementary data associated with this article can be found, in the online version, at doi:10.1016/j.jhep.2008.07.036.

References

[1] El-Serag HB, Mason AC. Rising incidence of hepatocellular carcinoma in the United States. N Engl J Med 1999;340:745–750.
[2] Bosch FX, Ribes J, Diaz M, Cleries R. Primary liver cancer: worldwide incidence and trends. Gastroenterology 2004;127:S5–S16.
[3] Wang XW, Hussain SP, Huo TI, Wu CG, Forgues M, Hofseth LJ, et al. Molecular pathogenesis of human hepatocellular carcinoma. Toxicology 2002;181-182:43–47.
[4] Yamashita T, Kaneko S, Hashimoto S, Sato T, Nagai S, Toyoda N, et al. Serial analysis of gene expression in chronic hepatitis C and hepatocellular carcinoma. Biochem Biophys Res Commun 2001;282:647–654.
[5] Shirota Y, Kaneko S, Honda M, Kawai HF, Kobayashi K. Identification of differentially expressed genes in hepatocellular carcinoma with cDNA microarrays. Hepatology 2001;33:832–840.
[6] Okabe H, Satoh S, Kato T, Kitahara O, Yanagawa R, Yamaoka Y, et al. Genome-wide analysis of gene expression in human hepatocellular carcinomas using cDNA microarray: identification of genes involved in viral carcinogenesis and tumor progression. Cancer Res 2001;61:2129–2137.
[7] Xu XR, Huang J, Xu ZG, Qian BZ, Zhu ZD, Yan Q, et al. Insight into hepatocellular carcinogenesis at transcriptome level by comparing gene expression profiles of hepatocellular carcinoma with those of corresponding noncancerous liver. Proc Natl Acad Sci USA 2001;98:15089–15094.
[8] Iizuka N, Oka M, Yamada-Okabe H, Mori N, Tamesa T, Okada T, et al. Comparison of gene expression profiles between hepatitis B virus- and hepatitis C virus-infected hepatocellular carcinoma by oligonucleotide microarray data on the basis of a supervised learning method. Cancer Res 2002;62:3939–3944.
[9] Thorgeirsson SS, Grisham JW. Molecular pathogenesis of human hepatocellular carcinoma. Nat Genet 2002;31:339–346.
[10] Lee JS, Thorgeirsson SS. Genome-scale profiling of gene expression in hepatocellular carcinoma: classification, survival prediction, and identification of therapeutic targets. Gastroenterology 2004;127:S51–S55.
[11] Suriawinata A, Xu R. An update on the molecular genetics of hepatocellular carcinoma. Semin Liver Dis 2004;24:77–88.
[12] El-Serag HB, Tran T, Everhart JE. Diabetes increases the risk of chronic liver disease and hepatocellular carcinoma. Gastroenterology 2004;126:460–468.
[13] Hassan MM, Hwang LY, Hatten CJ, Swaim M, Li D, Abbruzzese JL, et al. Risk factors for hepatocellular carcinoma: synergism of alcohol with viral hepatitis and diabetes mellitus. Hepatology 2002;36:1206–1213.
[14] Ohata K, Hamasaki K, Toriyama K, Matsumoto K, Saeki A, Yanagi K, et al. Hepatic steatosis is a risk factor for hepatocellular carcinoma in patients with chronic hepatitis C virus infection. Cancer 2003;97:3036–3043.
[15] Calle EE, Rodriguez C, Walker-Thurmond K, Thun MJ. Overweight, obesity, and mortality from cancer in a prospectively studied cohort of US adults. N Engl J Med 2003;348:1625–1638.
[16] Walsh MJ, Vanags DM, Clouston AD, Richardson MM, Purdie DM, Jonsson JR, et al. Steatosis and liver cell apoptosis in chronic hepatitis C: a mechanism for increased liver injury. Hepatology 2004;39:1230–1238.

[17] Powell EE, Jonsson JR, Clouston AD. Steatosis: co-factor in other liver diseases. Hepatology 2005;42:5–13.
[18] Velculescu VE, Zhang L, Vogelstein B, Kinzler KW. Serial analysis of gene expression. Science 1995;270:484–487.
[19] Yamashita T, Hashimoto S, Kaneko S, Nagai S, Toyoda N, Suzuki T, et al. Comprehensive gene expression profile of a normal human liver. Biochem Biophys Res Commun 2000;269:110–116.
[20] Desmet VJ, Gerber M, Hoofnagle JH, Manns M, Scheuer PJ. Classification of chronic hepatitis: diagnosis, grading and staging. Hepatology 1994;19:1513–1520.
[21] Polyak K, Xia Y, Zweier JL, Kinzler KW, Vogelstein B. A model for p53-induced apoptosis. Nature 1997;389:300–305.
[22] Yokoyama C, Wang X, Briggs MR, Admon A, Wu J, Hua X, et al. SREBP-1, a basic-helix–loop-helix–leucine zipper protein that controls transcription of the low density lipoprotein receptor gene. Cell 1993;75:187–197.
[23] Wang HC, Chang WT, Chang WW, Wu HC, Huang W, Lei HY, et al. Hepatitis B virus pre-S2 mutant upregulates cyclin A expression and induces nodular proliferation of hepatocytes. Hepatology 2005;41:761–770.
[24] Takeba Y, Kumai T, Matsumoto N, Nakaya S, Tsuzuki Y, Yanagida Y, et al. Irinotecan activates p53 with its active metabolite, resulting in human hepatocellular carcinoma apoptosis. J Pharmacol Sci 2007;104:232–242.
[25] Closset J, Van de Stadt J, Delhaye M, El Nakadi I, Lambilliotte JP, Gelin M. Hepatocellular carcinoma: surgical treatment and prognostic variables in 56 patients. Hepatogastroenterology 1999;46:2914–2918.
[26] Arsura M, Cavin LG, Calvisi DF, Thorgeirsson SS, Eferl R, Ricci R, et al. Nuclear factor-kappaB and liver carcinogenesis. Cancer Lett 2005;229:157–169.
[27] Calvisi DF, Thorgeirsson SS. Molecular mechanisms of hepatocarcinogenesis in transgenic mouse models of liver cancer. Toxicol Pathol 2005;33:181–184.
[28] Eferl R, Ricci R, Kenner L, Zenz R, David JP, Rath M, et al. Liver tumor development. c-Jun antagonizes the proapoptotic activity of p53. Cell 2003;112:181–192.
[29] Xu L, Hui L, Wang S, Gong J, Jin Y, Wang Y, et al. Expression profiling suggested a regulatory role of liver-enriched transcription factors in human hepatocellular carcinoma. Cancer Res 2001;61:3176–3181.
[30] Horton JD, Goldstein JL, Brown MS. SREBPs: activators of the complete program of cholesterol and fatty acid synthesis in the liver. J Clin Invest 2002;109:1125–1131.
[31] Yahagi N, Shimano H, Hasegawa K, Ohashi K, Matsuzaka T, Najima Y, et al. Co-ordinate activation of lipogenic enzymes in hepatocellular carcinoma. Eur J Cancer 2005;41:1316–1322.
[32] Kawaguchi K, Honda M, Yamashita T, Shirota Y, Kaneko S. Differential gene alteration among hepatoma cell lines demonstrated by cDNA microarray-based comparative genomic hybridization. Biochem Biophys Res Commun 2005;329:370–380.
[33] Van de Sande T, De Schrijver E, Heyns W, Verhoeven G, Swinnen JV. Role of the phosphatidylinositol 3′-kinase/PTEN/Akt kinase pathway in the overexpression of fatty acid synthase in LNCaP prostate cancer cells. Cancer Res 2002;62:642–646.
[34] Yang YA, Han WF, Morin PJ, Chrest FJ, Pizer ES. Activation of fatty acid synthesis during neoplastic transformation: role of mitogen-activated protein kinase and phosphatidylinositol 3-kinase. Exp Cell Res 2002;279:80–90.
[35] You M, Fischer M, Deeg MA, Crabb DW. Ethanol induces fatty acid synthesis pathways by activation of sterol regulatory element-binding protein (SREBP). J Biol Chem 2002;277:29342–29347.
[36] Muller-Wieland D, Kotzka J. SREBP-1: gene regulatory key to syndrome X? Ann NY Acad Sci 2002;967:19–27.
[37] Sekiya M, Yahagi N, Matsuzaka T, Najima Y, Nakakuki M, Nagai R, et al. Polyunsaturated fatty acids ameliorate hepatic steatosis in obese mice by SREBP-1 suppression. Hepatology 2003;38:1529–1539.
[38] Marrero JA, Fontana RJ, Su GL, Conjeevaram HS, Emick DM, Lok AS. NAFLD may be a common underlying liver disease in patients with hepatocellular carcinoma in the United States. Hepatology 2002;36:1349–1354.
[39] Kim KH, Shin HJ, Kim K, Choi HM, Rhee SH, Moon HB, et al. Hepatitis B virus X protein induces hepatic steatosis via transcriptional activation of SREBP1 and PPARgamma. Gastroenterology 2007;132:1955–1967.
[40] Waris G, Felmlee DJ, Negro F, Siddiqui A. Hepatitis C virus induces proteolytic cleavage of sterol regulatory element binding proteins and stimulates their phosphorylation via oxidative stress. J Virol 2007;81:8122–8130.
[41] Furuta E, Pai SK, Zhan R, Bandyopadhyay S, Watabe M, Mo YY, et al. Fatty acid synthase gene is up-regulated by hypoxia via activation of Akt and sterol regulatory element binding protein-1. Cancer Res 2008;68:1003–1011.
[42] Tanaka N, Moriya K, Kiyosawa K, Koike K, Gonzalez FJ, Aoyama T. PPARalpha activation is essential for HCV core protein-induced hepatic steatosis and hepatocellular carcinoma in mice. J Clin Invest 2008;118:683–694.
[43] Kuhajda FP. Fatty acid synthase and cancer: new application of an old pathway. Cancer Res 2006;66:5977–5980.

Altered Hepatic Gene Expression Profiles Associated With Myocardial Ischemia

Hiroshi Ootsuji, MD; Masao Honda, MD, PhD; Shuichi Kaneko, MD, PhD; Soichiro Usui, MD, PhD; Masaki Okajima, MD, PhD; Hikari Okada, MS; Yoshio Sakai, MD, PhD; Toshinari Takamura, MD, PhD; Katsuhisa Horimoto, PhD; Masayuki Takamura, MD, PhD

Background—Acute coronary syndrome is sometimes accompanied by accelerated coagulability, lipid metabolism, and inflammatory responses, which are not attributable to the cardiac events alone. We hypothesized that the liver plays a pivotal role in the pathophysiology of acute coronary syndrome. We simultaneously analyzed the gene expression profiles of the liver and heart during acute myocardial ischemia in mice.

Methods and Results—Mice were divided into 3 treatment groups: sham operation, ischemia/reperfusion, and myocardial infarction. Mice with liver ischemia/reperfusion were included as additional controls. Marked changes in hepatic gene expression were observed after 24 hours, despite the lack of histological changes in the liver. Genes related to tissue remodeling, adhesion molecules, and morphogenesis were significantly upregulated in the livers of mice with myocardial ischemia/reperfusion or infarction but not in those with liver ischemia/reperfusion. Myocardial ischemia, but not changes in the hemodynamic state, was postulated to significantly alter hepatic gene expression. Moreover, detailed analysis of the signaling pathway suggested the presence of humoral factors that intervened between the heart and liver. To address these points, we used isolated primary hepatocytes and showed that osteopontin released from the heart actually altered the signaling pathways of primary hepatocytes to those observed in the livers of mice under myocardial ischemia. Moreover, osteopontin stimulated primary hepatocytes to secrete vascular endothelial growth factor-A, which is important for tissue remodeling.

Conclusions—Hepatic gene expression is potentially regulated by cardiac humoral factors under myocardial ischemia. These results provide new insights into the pathophysiology of acute coronary syndrome. **(*Circ Cardiovasc Genet.* 2010;3:68-77.)**

Key Words: coronary disease ■ genetics ■ liver ■ myocardial infarction

In addition to chest pain, acute coronary syndrome (ACS) is sometimes accompanied by systemic manifestations, such as proinflammatory responses, activation of the coagulation-fibrinolytic system, and lipid metabolism.[1–3] These are considered to be systemic reactions involving multiple organs, which exacerbate the cardiac events.

Clinical Perspective on p 77

C-reactive protein, coagulation factors, and protein C, the levels of which fluctuate in ACS, are liver-specific factors. Although these reports were based on a limited number of factors, the observations suggest a close relation between the liver and myocardial ischemia and imply that the liver plays a pivotal role in the pathophysiology of ACS.

cDNA microarray technology allows simultaneous analysis of the expression levels of thousands of genes. Genome-based expression profiling provides useful information on the molecular pathogenesis of various diseases as well as disease progression and prognosis.[4–7] Previous microarray studies have examined the molecular dynamics of the myocardium induced by myocardial ischemia.[8,9] However, global gene expression analyses applied to the liver affected by myocardial ischemia have not been reported.

In this study, we examined the responses of hepatic gene expression to myocardial ischemia. Given the systemic inflammation that characterizes ACSs, we postulated that regulation of hepatic genes occurs by inflammatory mediators and not by alterations in hemodynamics or hepatic perfusion. Therefore, we used whole-genome transcriptional profiling to identify hepatic genes selectively regulated in myocardial ischemia.

Methods

This study was approved by institutional and governmental animal research committees and was conducted in accordance with the *Guide for the Care and Use of Laboratory Animals* published by the US National Institutes of Health (NIH publication No. 85-23, revised 1996). C57BL/6J mice (n=46; body weight, 24.1±1.4 g; 8 to 10

Received June 1, 2008; accepted November 10, 2009.

From the Department of Disease Control and Homeostasis (H. Ootsuji, M.H., S.K., S.U., M.O., H. Okada, Y.S., T.T., M.T.), Kanazawa University Graduate School of Medical Science, Kanazawa University, Kanazawa, Japan; and National Institute of Advanced Industrial Science and Technology (K.H.), Tokyo, Japan.

The online-only Data Supplement is available at http://circgenetics.ahajournals.org/cgi/content/full/CIRCGENETICS.108.795484.

Correspondence to Shuichi Kaneko, MD, PhD, Department of Disease Control and Homeostasis, Kanazawa University Graduate School of Medical Science, Kanazawa University, 13-1 Takara-machi, Kanazawa 920-8641, Japan. E-mail skaneko@m-kanazawa.jp

Circ Cardiovasc Genet **is available at http://circgenetics.ahajournals.org** **DOI: 10.1161/CIRCGENETICS.108.795484**

Table 1. Biochemical Assessment

		6 h				24 h			
	Before Operation	Sham	I/R	Infarction	Liver I/R	Sham	I/R	Infarction	Liver I/R
No.	5	5	5	5	5	6	5	5	5
CPK, U/L	944±98	5031±646	11597±1272*	19830±1154*	8673±1379	1702±181	1913±184	2939±515†	1595±349
AST, U/L	94±4	674±41	899±21*	1858±59*	414±43	200±19	277±14	661±28*	163±22
ALT, U/L	58±4	119±9	115±6	153±7	143±18	46±3	64±6	107±11*	42±3
LDH, U/L	652±32	2684±206	3432±80†	5264±111*	2478±446	681±72	867±37	2095±164*	862±209

Values are presented as mean±SE. CPK indicates creatine kinase; AST, aspartate aminotransferase; ALT, alanine aminotransferase; and LDH, lactate dehydrogenase.

*$P<0.01$ compared with sham.

†$P<0.05$ compared with sham.

weeks of age; Charles River Laboratories, Yokohama, Japan) were divided into the following treatment groups: sham operation (n=11), ischemia/reperfusion (I/R; n=10), myocardial infarction (MI; n=10), liver I/R (n=10), and sham operation plus hydralazine (n=5). Hepatic gene expression was evaluated among these groups, and the results were further investigated in primary mouse hepatocytes.

Additional Methods

An expanded Methods section containing details of animal surgery, hydralazine group, liver I/R group, blood sampling and analysis, histopathological analysis, blood pressure and heart rate measurements, microarray experiments, processing of cDNA microarray data, extraction of significantly upregulated cardiac and hepatic genes, pathway analysis, ELISA for secreted osteopontin and vascular endothelial growth factor (*VEGF*), primary hepatocyte experiments, and quantitative real-time detection polymerase chain reaction (RTD-PCR) is available in the online-only Data Supplement.

All microarray data have been deposited in the National Center for Biotechnology Information Gene Expression Omnibus database with the series accession number GSE14843.

Data Analysis

The data are presented as the mean±SEM for each group of mice and were analyzed by ANOVA with Bonferroni post hoc test for multiple comparisons. Statistical analyses of blood sampling, blood pressure, and heart rate were performed with the Steel (heterogeneity of variance) multicomparison test. Significance was set at $P<0.05$. Statistical analyses were performed with SAS statistical software (SAS Institute Japan, Tokyo, Japan).

Results

Establishment of Cardiac I/R or MI in Mice

Cardiac I/R or MI was successfully induced in normal C57BL/6J mice. The levels of cardiac enzymes, such as creatine kinase, aspartate aminotransferase, and lactate dehydrogenase, increased significantly after 6 hours in the I/R group and showed markedly greater increases in the infarction group compared with the sham group (Table 1). In addition, the normalization of these enzyme levels was reduced after 24 hours in the infarction group.

Histologically, azan or hematoxylin/eosin staining showed wall thinning, coagulation necrosis, and transmural fibrosis in the risk area in the infarction group but not in the I/R group (data not shown). As shown in Table 2, no significant differences were found in heart rate or blood pressure after 24 hours compared with the preoperative values in the sham and I/R groups, whereas a decrease in blood pressure was found in the infarction group.

Histological Assessment of the Liver After Cardiac I/R or MI

The I/R and infarction groups showed a minimal, but transient, increase in alanine aminotransferase ALT. Although alanine aminotransferase may be released from the myocardium[10] rather than from the liver, to exclude the effect of the transient change in hepatic venous pressure associated with cardiogenic shock, we examined histological changes in the liver after myocardial I/R or infarction. No histological abnormalities were observed in the shocked liver, as indicated by the lack of hepatocyte necrosis in acinar zone 3 in the sham, I/R, and infarction groups (Figure 1a, 1c, 1e, and 1g; hematoxylin/eosin staining). In addition, no signs of liver congestion were observed, as indicated by the lack of dilatation of the terminal hepatic venules and adjacent sinusoids in the sham, I/R, or infarction group (Figure 1b, 1d, 1f, and 1h; silver staining).

On transmission electron microscopy, no ischemic changes, such as swelling or loss of cristae in the mitochondria, a mixed irregular pattern or swelling of the rough endoplasmic reticulum, or dilatation or indistinct appearance of the sinusoids, were observed in the sham, I/R, or infarction group (Figure 2A through 2C). Based on these results, histological analysis did not demonstrate the presence of shock or congestive liver in the I/R or infarction group.

Changes in the Hepatic Gene Expression Profile After Cardiac I/R or MI

Although no histological changes were observed in the liver after cardiac I/R or MI, significant changes in gene expression were noted. Hierarchical clustering analysis, which is a nonsupervised learning method that includes 23 281 nonfil-

Table 2. HR, sBP, and mBP

		24 h		
	Before Operation	Sham	I/R	Infarction
HR, bpm	575±27	553±30	553±27	568±16
sBP, mm Hg	105±2	102±2	95±1	80±4*
mBP, mm Hg	78±3	74±2	63±2	56±4†

Values are presented as mean±SE. HR indicates heart rate; sBP, systolic blood pressure; and mBP, mean blood pressure.

*$P<0.01$ compared with sham.

†$P<0.05$ compared with sham.

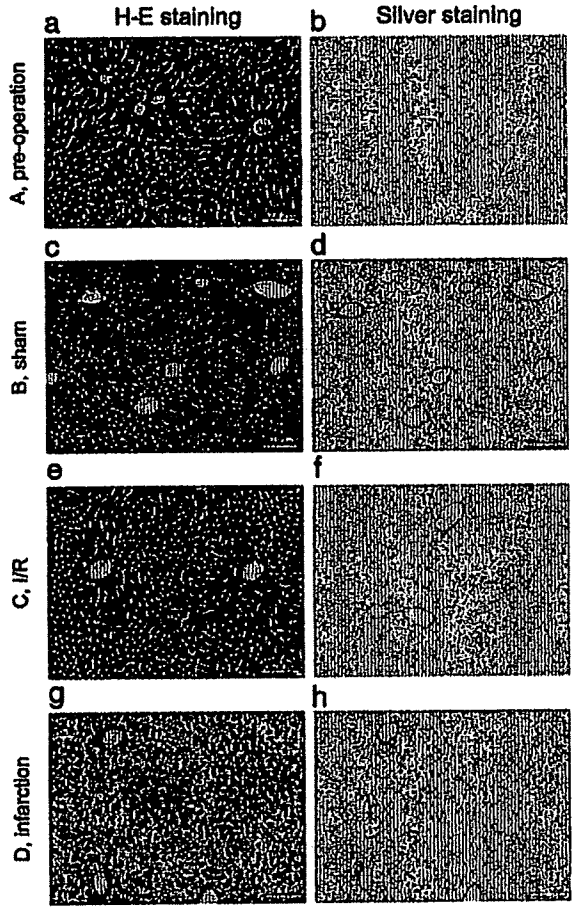

Figure 1. Histological comparison of hematoxylin/eosin staining and silver staining of the liver after 24 hours. Preoperation (A), sham (B), I/R (C), and infarction (D). Scale bars represent 100 μm. Hematoxylin/eosin staining (a, c, e, and g); silver staining (b, d, f, and h). No indication of shock or congestive liver was observed in any group (magnification, ×200).

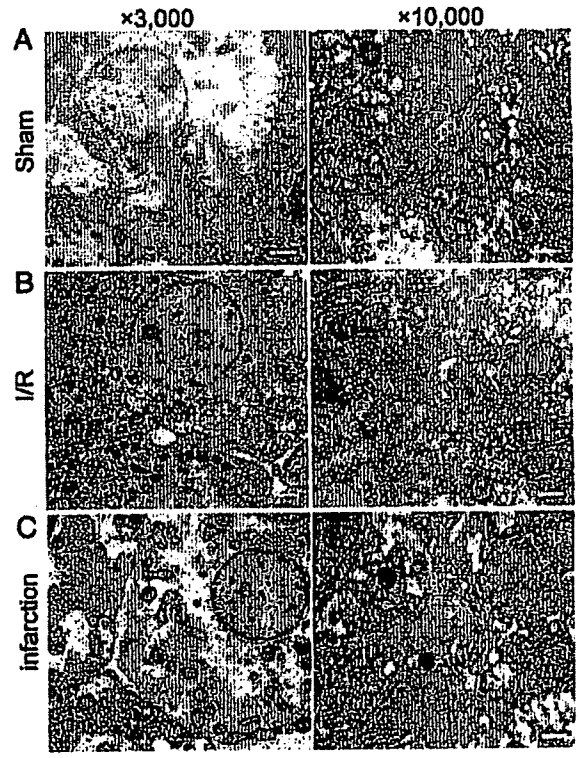

Figure 2. Representative electron microphotographs of the liver after 24 hours. Sham (A), I/R (B), and infarction (C). Scale bars represent 2 μm on the left (magnification, ×3000) and 500 nm on the right (magnification, ×10 000). No indication of shocked liver was observed in any group. M indicates mitochondria; rER, rough endoplasmic reticulum; B, bile canaliculi; N, nucleus.

tered genes, produced clusters for the I/R or infarction group and the sham-operated group (data not shown). Because nonfiltered genes may include those that are unchanged in all samples, which generated "noise" that prevented efficient gene clustering, we filtered out these genes with different stringency and performed hierarchical clustering. Hierarchical clustering with 9165 (log-ratio variations >40th percentile) or 5156 (log-ratio variations >50th percentile) filtered genes clearly demonstrated clusters for the I/R or infarction group after 24 hours, for the I/R or infarction group after 6 hours, and for the sham group after 6 and 24 hours (supplemental Figure I). Hierarchical clustering with 773 (log-ratio variations >80th percentile) or 96 (log-ratio variations >90th percentile) filtered genes showed more detailed and clearer clusters for the I/R group after 24 hours, for the infarction group after 24 hours, for the I/R or infarction group after 6 hours, and for the sham group after 6 and 24 hours (Figure 3). Thus, by filtering out "noise" genes, more detailed and clearer clustering could be obtained, thus addressing the reliability of the analysis.[11] The increased robustness (R-index) and decreased discrepancy (D-index) of clustering with filtering conditions supported this finding (supplemental Figure I; expanded Methods and Results).

Class prediction analysis, a supervised learning method based on the compound covariate predictor, was performed with various clinical parameters, including provocation (I/R or infarction), 6 hours (I/R or infarction after 6 hours), 24 hours (I/R or infarction after 24 hours), and time (sham or 6 hours, sham or 24 hours, and 6 or 24 hours). The results

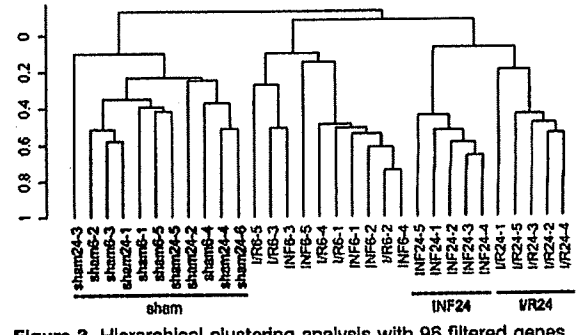

Figure 3. Hierarchical clustering analysis with 96 filtered genes (genes with log-ratio variation in the 90th percentile and data missing >5% were excluded). The resulting dendrogram shows clear clusters for the I/R group after 24 hours, the infarction group after 24 hours, and the sham group after 6 and 24 hours.

Table 3. Class Prediction Analysis (Supervised Learning Methods)

Classifier Category	Clinical Group	Total No. of Classes	No. of Cases Misclassified	Classifier *P*	Mean Percent of Correct Classification	No. of Genes in the Classifiers ($P<0.002$)
Provocation	I/R	10	2	0.02	80	85
	INF	10	2			
6 h	I/R	5	2	0.48	50	23
	INF	5	3			
24 h	I/R	5	0	0.015	100	218
	INF	5	0			
Time	Sham	11	0	0.001	90	644
	6 h	10	2			
	Sham	11	0	<0.0005	95	3380
	24 h	10	1			
	6 h	10	1	0.004	85	747
	24 h	10	2			

INF indicates infarction.

indicated that provocation, 24 hours, and time significantly classified these models (Table 3).

Both nonsupervised and supervised learning methods indicated differences in hepatic gene expression profiling among sham, 6 hours, and 24 hours after heart provocation, and different heart provocation (I/R or infarction) may generate differences in hepatic gene expression, especially 24 hours after provocation.

Identification of Genes Differentially Expressed Between I/R and Infarction

Because the filtering process may result in loss of important genes, for identification of differentially expressed genes among different groups, we used a class comparison analysis tool (http://linus.nci.nih.gov/BRB-ArrayTools.html). Class comparison analysis ($P<0.0005$) among the 5 groups (ie, sham, I/R-6, I/R-24, infarction-6, and infarction-24) was performed, and genes that were differentially expressed among the 5 groups were extracted. On 1-way hierarchical clustering analysis of the extracted genes and heat map, 6 gene clusters were assigned on the basis of the gene expression patterns (Figure 4). Of the 6 groups, group 2 showed significant upregulation for I/R and infarction after 24 hours compared with the other groups. Group 3 showed upregulation for I/R, but not for infarction, after 24 hours. Group 4 showed downregulation for I/R and infarction after 24 hours compared with the other groups. Group 5 showed downregulation for infarction after 24 hours compared with the other groups. Representative genes (>3-fold difference in *t* value) and frequent pathways observed in each group (based on the MetaCore database) are listed in supplemental Tables I through IV.

Interestingly, in group 2, genes related to tissue remodeling, adhesion molecules, and morphogenesis were significantly upregulated. This may be related to the induction of tissue repair factors, such as antigenic factor and myocardiogenic factors, associated with I/R or infarction. In addition, genes involved in the cell cycle and apoptosis and neuron-related genes, such as retinoblastoma 1, angiopoietin-like 4, apoptotic peptidase-activating factor 1, transformation-related protein 53 (*p53*), and Eph receptor B1, were preferentially expressed. The expression of group 2 genes was significantly correlated with serum creatine kinase levels, suggesting that these genes reflect the severity of cardiac damage. Especially, ($R=0.856$, $P<e^{-07}$) and apoptotic peptidase-activating factor 1 ($R=0.856$, $P<e^{-07}$) were highly correlated with creatine kinase (supplemental Table I).

In group 3, in addition to the genes described earlier, chemokine and hormone gene pathways involved in interleukin (IL)-8 and androgen or estrogen receptor signaling were upregulated, suggesting that more tissue repair and bioreactive signaling pathways were activated. This may reflect the presence of a living myocyte I/R condition. In group 4, genes involved in lipid catabolism, immune response, proteolysis, and oxidative stress, such as apolipoprotein A-II, CD7 antigen, and reduced nicotinamide-adenine dinucleotide phosphate oxidase 1, were downregulated in the infarction and I/R groups after 24 hours. In group 5, genes involved in muscle and neurite morphogenesis, such as myosin (heavy polypeptide 11, smooth muscle) and ephrin A5, were significantly downregulated in the infarction group after 24 hours.

Effects of Hemodynamic State on Hepatic Gene Expression Profile

To exclude the possibility that changes in hemodynamic state induced alterations in hepatic gene expression, we examined the livers of mice subjected to liver I/R. For liver I/R, gentle occlusion of the hepatic artery and portal vein was applied so that the extent of liver injury was comparable with those in the myocardial I/R and infarction models (Table 1).

We analyzed the gene expression profile of the liver I/R group by using the same extracted genes as shown in Figure 4. The gene expression patterns induced in the myocardial I/R and infarction groups are clearly different from those in the liver I/R group (Figure 5), except for the group 3 gene cluster in myocardial I/R. It should be noted that the group 3 gene cluster was upregulated in the myocardial I/R group at 24

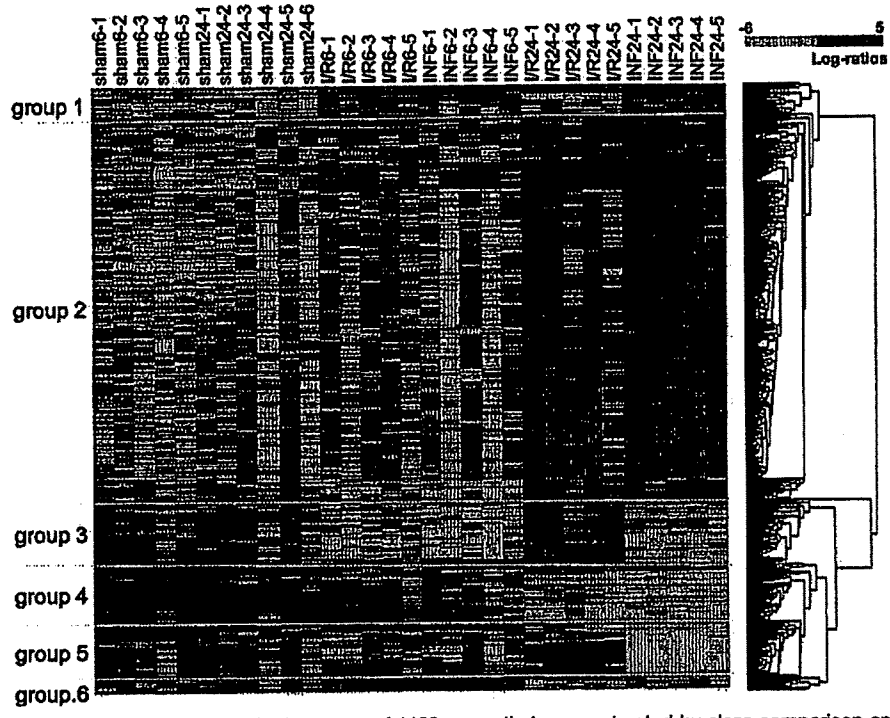

Figure 4. One-way hierarchical clustering and a heat map of 1166 genes that were extracted by class comparison analysis ($P<0.0005$). Each column corresponds to a sample, and each row represents a gene. The gene cluster data are graphically presented as colored images: red indicates upregulated genes, and green indicates downregulated genes. The genes with the most similar patterns of expression are adjacent to one another. Detailed definitions of each group are given in the text. Representative genes and frequently observed pathways are listed in supplemental Tables I through IV.

hours after provocation, whereas it was upregulated from 6 hours after provocation in the liver I/R group. Therefore, the delayed changes in hepatic gene expression in the myocardial I/R and infarction models may be due to different mechanisms resulting from liver I/R.

The assessment of liver weight revealed no differences between the myocardial I/R and infarction groups (supplemental Table V). This result supports our histological findings and indicates an absence of liver congestion in the myocardial I/R and infarction groups.

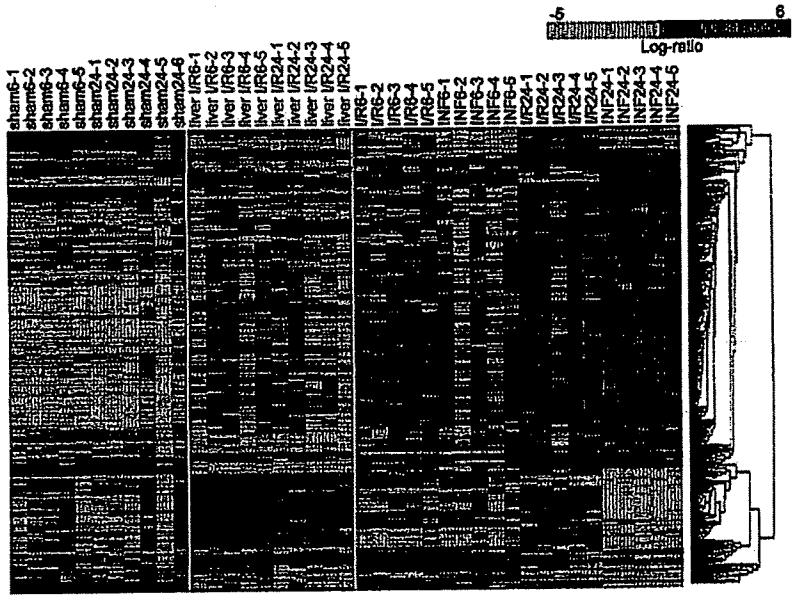

Figure 5. One-way hierarchical clustering and a heat map of the liver I/R group and others with the same extracted genes as shown in Figure 4. Each column corresponds to a sample, and each row represents a gene. The gene cluster data are graphically presented as colored images: red indicates upregulated genes, and green indicates downregulated genes. The genes with the most similar patterns of expression are adjacent to one another. Gene expression patterns induced in the liver I/R group clearly differed from those in the myocardial I/R and infarction groups.

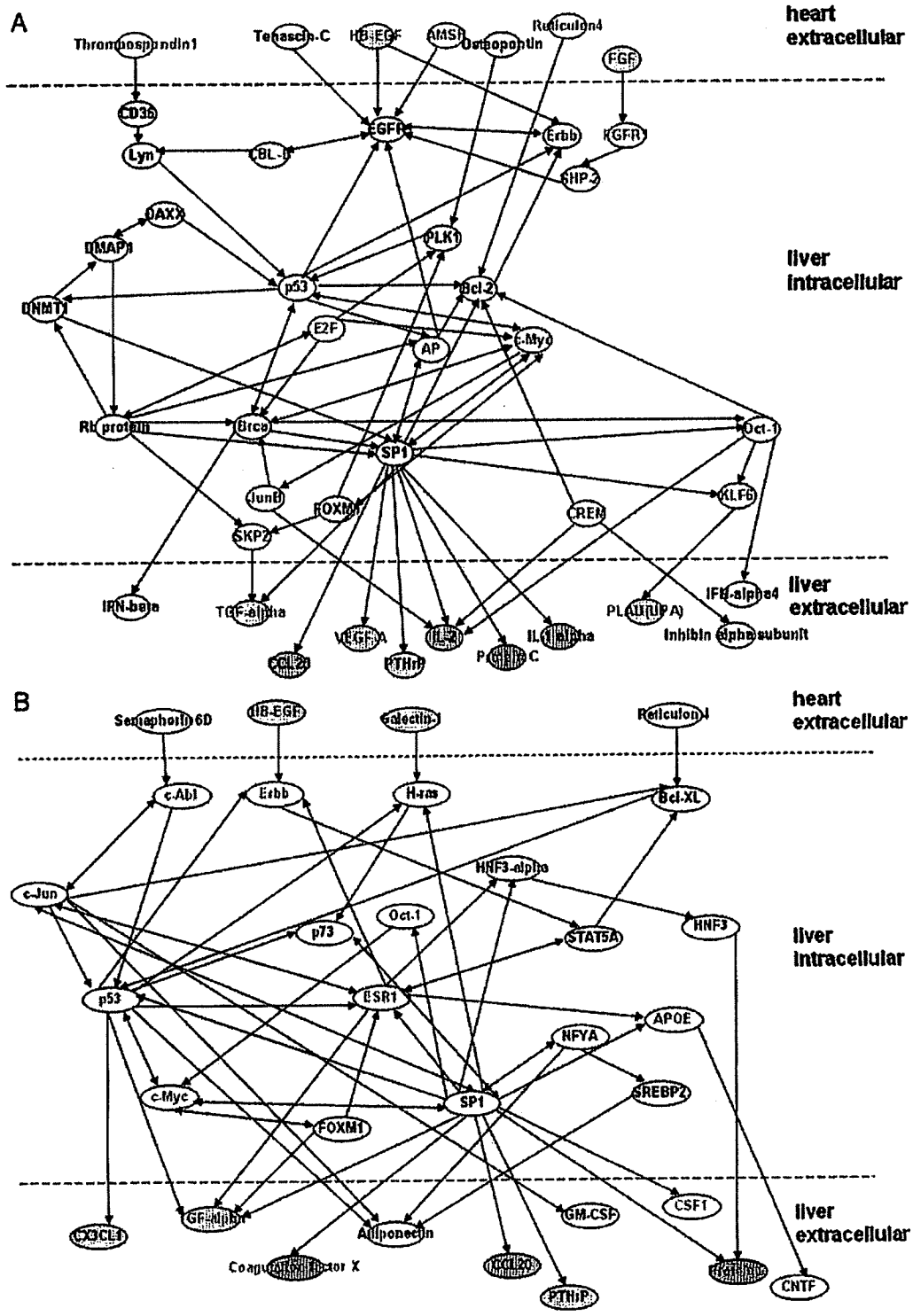

Figure 6. A, Postulated gene network of differentially expressed genes in infarction. B, Postulated gene network of differentially expressed genes in I/R. Detailed definitions of heart-extracellular, liver-intracellular, and liver-extracellular are given in the Methods. Yellow ovals indicate genes related to angiogenesis; green ovals, genes related to coagulation-fibrinolysis; blue ovals, genes related to inflammation; and red characters, genes upregulated in microarray analysis of primary hepatocytes treated with osteopontin. The network diagrams consist of representative genes. All abbreviations are defined in supplemental Tables VI through XI.

Detailed Gene Network Analysis Between the Liver and Heart in Myocardial Ischemia

Several factors can affect the liver, including humoral factors released from the ischemic myocardium, the hemodynamic state, or the autonomic nervous system. We focused on the possibility that humoral factors released from the heart may affect the liver. Cardiac gene expression profiles induced by myocardial ischemia were investigated to identify cardiac genes affecting the liver. To obtain a detailed and comprehensive gene network for the liver and heart, individual data from the liver after 24 hours were integrated with pooled data from the risk area and nonrisk area of the heart. Initially, we divided the heart and liver genes into 3 groups: heart-extracellular, liver-intracellular, and liver-extracellular. To find the network among these induced genes, published results for the interactions of individual genes were integrated with these results by using MetaCore software (GeneGo, St. Joseph, Mich). Direct interactions between individual genes were sought. Genes were excluded according to the following criteria: (1) heart-extracellular, no output signal into liver-intracellular; (2) liver-intracellular, no bidirectional signals; and (3) liver-extracellular, no input signal from liver-intracellular. As expected, the network of these differentially expressed genes involved complex interactions of individual genes; however, representative signaling pathways for MI or I/R injury were identified (Figure 6).

During MI, fibroblast growth factor, osteopontin, and heparin-binding epidermal growth factor-like growth factor (*HB-EGF*) were upregulated in the heart and may have been systemically secreted. Endothelial growth factor receptor and fibroblast growth factor receptor-1 may play important roles in receiving these signals in the liver. Transcription factors such as *p53*, myelocytomatosis oncogene, *trans*-acting transcription factor 1, and octamer-binding transcription factor 1 are important molecules in the regulation of these signaling pathways. Protein C, VEGF-A, and urokinase were expected to be systemically secreted from the liver (supplemental Tables VI through VIII). After infarction, genes involved in inflammation, the coagulation-fibrinolytic system, and angiogenesis showed preferential expression. After I/R, heparin-binding epidermal growth factor was upregulated in the heart and was expected to be systemically secreted. V-*erb*-a erythroblastic leukemia viral oncogene homolog 4 (avian) may play an important role in receiving these signals in the liver. Transcription factors such as *trans*-acting transcription factor 1, *p53*, estrogen receptor-1α, and signal transducer and activator of transcription 5A are potentially important molecules for regulation of these signaling pathways. Protein C, coagulation factor X, ciliary neurotrophic factor, and colony-stimulating factor-1 (macrophage) (*CSF-1*) were expected to be systemically secreted from the liver. In I/R, angiogenesis-related genes were preferentially upregulated (supplemental Tables IX through XI). On comparison of the expression profiles of the heart and liver, genes expressed at significantly higher levels in the heart than in the liver were designated as He, and those expressed at significantly higher levels in the liver than in the heart were designated as Li. Genes expressed in both the heart and liver were described as He/Li (supplemental Tables VIII and XI). In this analysis, most of the factors that were expected to be secreted from the liver induced by I/R and infarction were liver-specific. Most of these genes were not significantly upregulated in the liver I/R groups.

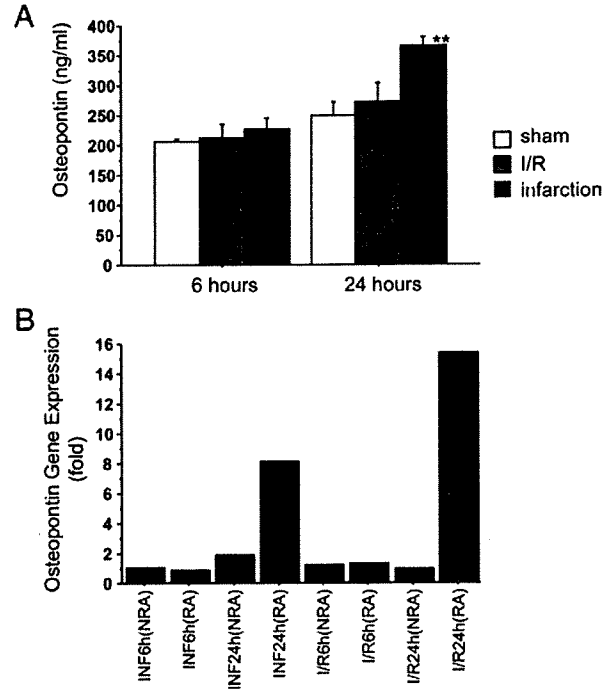

Figure 7. A, The time course of the serum osteopontin concentrations in sham, I/R, and infarction groups. The assessment of serum osteopontin by ELISA in the sham, I/R, and infarction groups after 6 and 24 hours. The serum concentrations of osteopontin after 24 hours were 365.7±14.6 ng/mL, 273.0±30.6 ng/mL, and 249.2±23.4 ng/mL in infarction, I/R, and sham groups, respectively. Error bars represent the SEM. $^{**}P<0.01$ compared with sham. B, The changes in osteopontin gene expression in the infarcted and reperfused heart. INF indicates infarction; NRA, nonrisk area; RA, risk area.

Serum Osteopontin Concentrations in Mice

Of the infarction-induced, cardiac-secreted factors that were expected to stimulate multiple liver genes, we quantified the serum levels of osteopontin by ELISA. Serum osteopontin concentration was significantly increased in the infarction group compared with the sham group ($P=0.0012$) after 24 hours (Figure 7A). In addition, the changes in osteopontin gene expression in the infarcted and reperfused heart are shown in Figure 7B.

Signaling Pathway in Primary Hepatocytes Treated With Osteopontin

To determine whether ischemia-induced, cardiac-secreted factors affected hepatic gene expression, we investigated the effects of osteopontin on primary mouse hepatocytes (supplemental Materials and Methods); 979 genes were upregulated and 734 genes were downregulated ($P<0.05$ and fold change >2.0 determined by class comparison analysis) by osteopontin in primary hepatocytes (GSE14843). The most frequent pathway processes observed among upregulated genes as determined with the use of MetaCore software are

shown in supplemental Table XII. Osteopontin upregulated signaling pathways of protein C, angiogenesis, cell adhesion, etc, which were observed in groups 2 and 3 gene clusters in the mouse liver under conditions of myocardial ischemia (Figure 4; supplemental Tables I and II). The role of osteopontin in the postulated gene network connecting the liver and heart in myocardial ischemia is shown in Figure 6. Interestingly, many of the genes included in the postulated gene network were actually activated by osteopontin ($P<0.05$ or fold change >2.0 by class comparison analysis) in primary hepatocytes. Unexpectedly, osteopontin activated *HB-EGF*, thrombospondin 1, and fibroblast growth factor, which were released from the ischemic heart (Figure 6; supplemental Table VI) in primary hepatocytes. These results indicated that these proteins were released from the liver and from the heart under conditions of myocardial ischemia through osteopontin, and an autocrine signaling pathway may exist in the liver.

Among the candidate hepatic-secreted factors under conditions of myocardial ischemia (Figure 6A; supplemental Table VIII), we quantified the levels of *VEGF-A* in the supernatants of primary hepatocytes treated with osteopontin. The concentration of *VEGF-A* measured by ELISA was significantly increased in the supernatants of primary hepatocytes treated with osteopontin (n=6) compared with the mock group (n=7; $P=0.0042$; supplemental Figure II). Thus, important factors for tissue remodeling could be released from the liver through humoral factors, such as osteopontin, that are released from the heart under conditions of myocardial ischemia.

Quantitative RTD-PCR

We performed a quantitative RTD-PCR with TaqMan probes. In the I/R group, protein C, coagulation factor X, *CNTF*, and *CSF-1* were upregulated in the liver. In the infarction group, protein C, urokinase, and *VEGF-A* were upregulated in the liver (supplemental Figure IIIA). In the hepatocytes treated with osteopontin, protein C, coagulation factor X, ciliary neurotrophic factor, *CSF-1*, urokinase, and *VEGF-A* were upregulated compared with the mock group (supplemental Figure IIIB). These results were consistent with those of cDNA microarray analyses performed in this study.

Discussion

The liver is an essential organ that synthesizes many bioactive proteins, including acute-phase inflammatory proteins (eg, C-reactive protein and IL-6) and coagulation factors. Therefore, it has been speculated that the liver may be involved in systemic reactions that modify the pathophysiology of ACS, although this possibility has not been addressed in detail.

In this study, we examined the gene expression profiles of the livers of mice affected by myocardial I/R or infarction. Marked changes in hepatic gene expression were observed after 24 hours, despite the lack of histological changes in the liver. These changes were essentially restored to normal after 3 to 7 days (data not shown). These findings may not be due to hemodynamic changes during myocardial I/R or infarction. Instead, inflammatory mediators or humoral factors released from the affected heart may be responsible for the observed alterations in hepatic gene expression. This was further confirmed by investigation of signaling pathways in primary hepatocytes induced by osteopontin, a candidate humoral factor released from the ischemic myocardium in vitro.

To exclude the possibility that these changes in gene expression were due to systemic hypotension during I/R or infarction, we performed an additional experiment involving liver I/R to examine whether a pattern of gene expression similar to that in the myocardial I/R and infarction groups could be observed in the liver. Hepatic gene expression in the liver I/R group was completely different from those in the myocardial I/R and infarction groups, with the exception of a small gene cluster (group 3). Although the group 3 gene cluster was upregulated in both the liver I/R and myocardial I/R groups at 24 hours after provocation, peak expression was delayed in the myocardial I/R group compared with the liver I/R group. A recent report of extended observations of cytokine expression in murine hepatic I/R injury indicated that the levels of expression of tumor necrosis factor-α, IL-1β, and IL-6 peaked within 4 hours and returned to baseline at 24 hours.[12] In contrast, in the myocardial I/R and infarction models, these cytokines peaked $\approx$24 to 48 hours and decreased at 7 days.[13] These findings were consistent with those of this study (data not shown). Therefore, the delayed peak of hepatic gene expression observed in this study may be correlated with the extent of inflammation in the myocardium after destruction of myocytes, rather than changes in the hemodynamic state of the liver. The lack of histological changes in the liver in the myocardial I/R and infarction models supported these suggestions, although the influence of hemodynamic state on hepatic gene expression should be carefully considered.

Interestingly, genes related to tissue remodeling, adhesion molecules, and morphogenesis were significantly upregulated in the livers of mice that were subjected to I/R or infarction. This may be related to the induction of tissue repair factors such as angiogenic or myocardiogenic factors in the heart undergoing I/R or infarction. In support of this notion, in addition to the genes upregulated during infarction, chemokines and hormonal factors, including IL-8, androgen, and estrogen receptor genes, were upregulated during I/R. These findings may reflect the presence of living myocytes and the greater release of tissue repair and bioreactive factors during I/R than during infarction.

A recent study that included a sequential analysis of ischemic mouse heart with quantitative RT-PCR demonstrated expression of IL-1β, IL-6, monocyte chemoattractant protein-1, macrophage inflammatory protein-1, and granulocyte-CSF at 6 and 24 hours.[13] These results were essentially consistent with those of our microarray analysis of pooled RNA extracted from heart specimens (data not shown).

In this study, the hepatic RNA samples were not pooled but were used to analyze the hepatic gene expression profiles individually. This strategy was successful, in that our microarray results were consistent with those produced from pooled or nonpooled liver specimens. Moreover, it facilitated the statistical evaluation of differentially expressed genes

among the various groups and revealed dynamic changes in hepatic gene expression through clustering analysis.

We analyzed the network connecting the heart-extracellular genes and liver-intracellular genes induced after I/R injury or infarction by using expression data from pooled heart samples and averaged the expression data for individual liver samples. The results suggested that factors secreted from the heart altered gene expression in the liver. By detailed analysis of signaling pathways, we identified 9 candidate genes (eg, *Osteopontin*, *HB-EGF*, *Reticulon 4*) that were upregulated in the heart and were expected to be systemically secreted and to regulate gene expression in the liver (Figure 6). Moreover, we identified the factors that were expected to be secreted from the liver induced by these signaling pathways, such as protein C, coagulation factor X, *CNTF*, *CSF-1*, and angiogenesis-related genes. These factors were expected to be systemically secreted from the liver and to modulate the pathophysiology and outcome of ACS. It has been reported that protein C prevents myocardial I/R injury,[14] *VEGF* enhances capillary density and improves cardiac function,[15] and urokinase is essential for cardiac functional recovery after acute myocardial infarction.[16]

Of the factors that were expected to be secreted from the heart, we confirmed that infarction increased the serum osteopontin concentration after 24 hours. Osteopontin is essential for the development of myocytes, tissue repair, and angiogenesis, and its downstream products, eg, polo-like kinase, were upregulated in the liver. To confirm these findings, we examined the signaling pathways in primary hepatocytes treated with osteopontin. Osteopontin activated signaling pathways of protein C, angiogenesis, and cell adhesion (supplemental Table XII) by inducing the expression of protein C, urokinase, *VEGF-A*, *CSF-1*, factor X, and ciliary neurotrophic factor (*CNTF*) in primary hepatocytes, which was confirmed by RTD-PCR or ELISA (supplemental Figures II and IIIB). Moreover, many other genes involved in the postulated gene network associating the liver and heart (Figure 6A and 6B) were actually activated in primary hepatocytes treated with osteopontin, confirming this signaling pathway. These results suggest that humoral factors play important roles in signal transduction from the ischemic myocardium to the liver.

Although our results addressed humoral factors from the heart that may affect hepatic gene expression, the effects of other factors, such as autonomic nerves, should also be considered. Because the liver has rich sympathetic and parasympathetic innervation,[17–19] it is possible that sympathetic hyperactivity affects hepatic gene expression. Although hydralazine has been reported to activate sympathetic nerves,[20,21] we observed no differences in gene expression in the hydralazine-treated group compared with the sham-operated group (data not shown). Therefore, autonomic nerves seemed to have little effect on hepatic gene expression determined in this study.

In conclusion, we reported new insights into the pathophysiology of ACS, which may facilitate identification of the mechanisms by which an acute coronary event causes systemic reactions. Further studies are needed to determine whether early therapeutic targeting of the liver during an acute coronary event has any beneficial effect on the clinical outcome in these patients.

Study Limitations

Although we confirmed that the serum osteopontin concentration was increased during myocardial ischemia, other proteins that could potentially be secreted from the heart and liver were not assayed. Further studies are needed to determine whether these proteins, including osteopontin, actually affect hepatic gene expression as observed in this study.

Acknowledgments

We thank Dr Yoh Zen (Department of Human Pathology, Kanazawa University Graduate School of Medical Science, Kanazawa, Japan) for consultation on the pathology of the liver.

Disclosures

None.

References

1. Pfohl M, Schreiber I, Liebich HM, Haring HU, Hoffmeister HM. Upregulation of cholesterol synthesis after acute myocardial infarction—is cholesterol a positive acute phase reactant? *Atherosclerosis*. 1999;142:389–393.
2. Tousoulis D, Antoniades C, Bosinakou E, Kotsopoulou M, Tsoufis C, Marinou K, Charakida M, Stefanadi E, Vavuranakis M, Latsios G, Stefanadis C. Differences in inflammatory and thrombotic markers between unstable angina and acute myocardial infarction. *Int J Cardiol*. 2007;115:203–207.
3. Busch G, Seitz I, Steppich B, Hess S, Eckl R, Schömig A, Ott I. Coagulation factor Xa stimulates interleukin-8 release in endothelial cells and mononuclear leukocytes: implications in acute myocardial infarction. *Arterioscler Thromb Vasc Biol*. 2005;25:461–466.
4. van't Veer LJ, Dai H, van de Vijver MJ, He YD, Hart AA, Mao M, Peterse HL, van der Kooy K, Marton MJ, Witteveen AT, Schreiber GJ, Kerkhoven RM, Roberts C, Linsley PS, Bernards R, Friend SH. Gene expression profiling predicts clinical outcome of breast cancer. *Nature*. 2002;415:530–536.
5. Nielsen TO, West RB, Linn SC, Alter O, Knowling MA, O'Connell JX, Zhu S, Fero M, Sherlock G, Pollack JR, Brown PO, Botstein D, van de Rijn M. Molecular characterization of soft tissue tumours: a gene expression study. *Lancet*. 2002;359:1301–1307.
6. van de Vijver MJ, He YD, van't Veer LJ, Dai H, Hart AA, Voskuil DW, Schreiber GJ, Peterse JL, Roberts C, Marton MJ, Parrish M, Atsma D, Witteveen A, Glas A, Delahaye L, van der Velde T, Bartelink H, Rodenhuis S, Rutgers ET, Friend SH, Bernards R. A gene-expression signature as a predictor of survival in breast cancer. *N Engl J Med*. 2002;347:1999–2009.
7. Hedenfalk I, Duggan D, Chen Y, Radmacher M, Bittner M, Simon R, Meltzer P, Gusterson B, Esteller M, Kallioniemi OP, Wilfond B, Borg A, Trent J, Raffeld M, Yakhini Z, Ben-Dor A, Dougherty E, Kononen J, Bubendorf L, Fehrle W, Pittaluga S, Gruvberger S, Loman N, Johannsson O, Olsson H, Sauter G. Gene-expression profiles in hereditary breast cancer. *N Engl J Med*. 2001;344:539–548.
8. Gabrielsen A, Lawler PR, Yongzhong W, Steinbrüchel D, Blagoja D, Paulsson-Berne G, Kastrup J, Hansson GK. Gene expression signals involved in ischemic injury, extracellular matrix composition and fibrosis defined by global mRNA profiling of the human left ventricular myocardium. *J Mol Cell Cardiol*. 2007;42:870–883.
9. LaFramboise WA, Bombach KL, Dhir RJ, Muha N, Cullen RF, Pogozelski AR, Turk D, George JD, Guthrie RD, Magovern JA. Molecular dynamics of the compensatory response to myocardial infarct. *J Mol Cell Cardiol*. 2005;38:103–117.
10. Giesen PL, Peltenburg HG, de Zwaan C, Janson PC, Flendrig JG, Hermens WT. Greater than expected alanine aminotransferase activities in plasma and in hearts of patients with acute myocardial infarction. *Clin Chem*. 1989;35:279–283.
11. Lu J, Getz G, Miska EA, Alvarez-Saavedra E, Lamb J, Peck D, Sweet-Cordero A, Ebert BL, Mak RH, Ferrando AA, Downing JR, Jacks T, Horvitz HR, Golub TR. MicroRNA expression profiles classify human cancers. *Nature*. 2005;435:834–838.
12. Langdale LA, Hoagland V, Benz W, Riehle KJ, Campbell JS, Liggitt DH, Fausto N. Suppressor of cytokine signaling expression with increasing

severity of murine hepatic ischemia-reperfusion injury. *J Hepatol.* 2008; 49:198–206.
13. Vandervelde S, van Luyn MJ, Rozenbaum MH, Petersen AH, Tio RA, Harmsen MC. Stem cell-related cardiac gene expression early after murine myocardial infarction. *Cardiovasc Res.* 2007;73:783–793.
14. Loubele ST, Spek CA, Leenders P, van Oerle R, Aberson HL, Hamulyák K, Ferrell G, Esmon CT, Spronk HM, ten Cate H. Activated protein C protects against myocardial ischemia/reperfusion injury via inhibition of apoptosis and inflammation. *Arterioscler Thromb Vasc Biol.* 2009;29: 1087–1092.
15. Zhang J, Ding L, Zhao Y, Sun W, Chen B, Lin H, Wang X, Zhang L, Xu B, Dai J. Collagen-targeting vascular endothelial growth factor improves cardiac performance after myocardial infarction. *Circulation.* 2009;119: 1776–1784.
16. Heymans S, Luttun A, Nuyens D, Theilmeier G, Creemers E, Moons L, Dyspersin GD, Cleutjens JP, Shipley M, Angellilo A, Levi M, Nübe O, Baker A, Keshet E, Lupu F, Herbert JM, Smits JF, Shapiro SD, Baes M, Borgers M, Collen D, Daemen MJ, Carmeliet P. Inhibition of plasminogen activators or matrix metalloproteinases prevents cardiac rupture but impairs therapeutic angiogenesis and causes cardiac failure. *Nat Med.* 1999;5:1135–1142.
17. Sasse D, Spornitz UM, Maly IP. Liver architecture. *Enzyme.* 1992; 46:8–32.
18. McCuskey RS, Reilly FD. Hepatic microvasculature: dynamic structure and its regulation. *Semin Liver Dis.* 1993;13:1–12.
19. Berthoud HR. Anatomy and function of sensory hepatic nerves. *Anat Rec A Discov Mol Cell Evol Biol.* 2004;280:827–835.
20. Yoshioka M, Togashi H, Minami M, Saito H. Effects of hydralazine on adrenal and cardiac sympathetic nerve activity in anesthetized rats. *Res Commun Chem Pathol Pharmacol.* 1986;54:313–320.
21. Johansson M, Elam M, Rundqvist B, Eisenhofer G, Herlitz H, Jensen G, Friberg P. Differentiated response of the sympathetic nervous system to angiotensin-converting enzyme inhibition in hypertension. *Hypertension.* 2000;36:543–548.

CLINICAL PERSPECTIVE

Acute coronary syndrome (ACS) is accompanied by systemic changes in inflammation, coagulation, and metabolism, which may affect the outcome and prognosis of ACS. These systemic reactions are not explained by cardiac events alone. Several lines of evidence suggest that patients with fatty liver disease have a high risk of developing cardiovascular diseases, and it is possible to speculate that the liver is involved in a systemic reaction that modifies the pathogenesis of ACS. However, the relation between liver and myocardial ischemia in the acute ischemic phase has not been elucidated so far. In this investigation, we simultaneously analyzed the gene expression profiles of the liver and heart during acute myocardial ischemia in mice and observed the presence of humoral factors that intervened between the heart and liver. These humoral factors were released from the heart and influenced the liver to secrete important tissue remodeling factors. One of these humoral factors, osteopontin, a widely expressed glycoprotein, was increased in the ischemic heart and altered the gene expression of hepatocytes to produce important tissue remodeling factors (such as vascular endothelial growth factor-A). Our observations suggest that hepatic gene expression is potentially regulated by humoral factors of cardiac origin provoked by myocardial ischemia, and we provide direct evidence that the liver is involved in a systemic reaction that accompanies ACS. Our findings provide potential new insights into the pathophysiology of ACS.

Screening of SMG7-Binding Peptides by Combination of Phage Display and Docking Simulation Analysis

Muhammed Zahed[1], Toshikazu Suzuki[1,*], Akiko Suganami[2], Hajime Sugiyama[3], Kazuo Harada[4], Masaki Takiguchi[3], Yutaka Tamura[2,*] and Nobuo Suzuki[1]

[1]*Department of Environmental Biochemistry, Graduate School of Medicine, Chiba University, Inohana, Chiba 260-8670, Japan;* [2]*Department of Bioinformatics, Graduate School of Medicine, Chiba University, Inohana, Chiba 260-8670, Japan;* [3]*Department of Biochemistry and Genetics, Graduate School of Medicine, Chiba University, Inohana, Chiba 260-8670, Japan;* [4]*Department of Life Sciences, Tokyo Gakugei University, Koganei, Tokyo 184-8501, Japan*

Abstract: We screened SMG7-binding peptides with phage display and docking simulation analysis. Although a consensus motif was absent in the phage display-derived candidates, we succeeded to find a peptide CDDRPPKSC, which can bind specifically to SMG7. We conclude that docking simulation helps to find high-affinity peptides efficiently, even if the phage display-screened candidates lack a consensus region.

Keywords: Phage display, *in silico* screening, docking simulation, pull-down assay.

INTRODUCTION

Phage display, the display of peptide or protein libraries on filamentous phages, has proved a rapid and successful method for obtaining peptides showing specific binding affinities or activities towards target proteins [1]. This technique is used in a number of applications including protein-protein interactions [2], monoclonal antibody development [3], target therapeutics [4], epitope mapping [5], finding novel proteins as diagnostic tools and in human therapeutics. Although this technique has shown success in developing consensus peptide sequences for target proteins, occasionally no consensus sequence is found among the candidate sequences, even if each of the candidates possess high affinity binding [6]. Some of the peptides may bind to different ligand epitopes, while others, though unrelated in primary sequence, may be similar in three-dimensional structure; still others may have novel binding structures. The existence of such molecules has already been demonstrated [7]. In this case, another selection method, in parallel with phage display, is necessary to find suitable candidate peptides from a structurally unrelated peptide pool.

Docking simulation analysis is a computer simulation of molecule-molecule interaction which allows the rapid and inexpensive prediction of candidate ligands from a pool of small molecules [8, 9]. When the higher order structure of the target protein is already known or can be predicted by homology modeling, docking simulation becomes the most useful virtual screening approach to identify the drugs candidates. Numerous successes of this approach for obtaining lead compounds for protein targets have been documented [10-12].

*Address correspondence to these authors at the Department of Environmental Biochemistry, Graduate School of Medicine, Chiba University, Inohana 1-8-1, Chuo-ku, Chiba 260-8670, Japan; Tel:/Fax: +81-43-226-2041; E-mail: piesuke@faculty.chiba-u.jp (T. Suzuki) and Department of Bioinformatics, Graduate School of Medicine, Chiba University, Inohana 1-8-1, Chuo-ku, Chiba 260-8670, Japan; Tel:/Fax: +81-43-226-2544; E-mail: yutaka_tamura@faculty.chiba-u.jp (Y. Tamura)

0929-8665/09 $55.00+.00

In the present study, we screened peptides binding specifically to the human SMG7 protein, a key player in the nonsense-mediated mRNA decay (NMD) pathway [13]. SMG7 has a structural similarity with human 14-3-3-ζ in its N-terminal domain [14]. High-affinity peptide antagonists of 14-3-3 have already been identified using phage display [15]. We thought that the isolation of small peptides that bind to N-terminal domain of SMG7 would provide antagonists; useful for further research of NMD pathway. However, peptide sequences in the candidate phage clones seemed to be random rather than sharing a consensus region. To find SMG7-binding peptide sequences from the candidates, we applied docking simulation analysis and ranked the strength of their possible binding affinity on the basis of docking energy. Furthermore, we determined the binding affinity of the *in silico*-selected peptides using an *in vitro* pull-down assay.

MATERIALS AND METHODS

Vector Construction

Full-length cDNA for human SMG7 (clone KIAA0250, accession No. D87437) was obtained from the Kazusa DNA research institute [16]. After constructing a *Bam* HI restriction enzyme site upstream of the initiation (AUG) codon of the cDNA, a 5kb DNA fragment containing the cDNA was inserted into the *Bam* HI site of pGEX-6P-1-GST fusion protein expression vector (GE Healthcare UK Limited, Buckinghamshire, UK), yielding pGEX-SMG7. To express the N-terminal half of the SMG7 protein, the C-terminal half of SMG7 cDNA was removed from pGEX-SMG7 by digestion with *Nde* I and *Xho* I and the larger fragment was self-ligated, yielding pGEX-SMG7 (*Nde* I).

Purification of Recombinant Protein

BL21 competent cells were transformed with pGEX-SMG7 (*Nde* I). The transformant was cultured in 2×YT medium containing 100 μg/ml ampicillin, and expression of glutathione S-transferase (GST)-SMG7 (Nde I) fusion pro-

tein was induced by isopropyl-1-thio-β-D-galactopyranoside. GST-SMG7 (Nde I) fusion protein was purified using a GSTrap FF column (GE Healthcare UK Limited). For phage biopanning assay, GST-SMG7 (Nde I) protein was digested overnight with PreScission Protease (GE Healthcare UK Limited) in the GSTrap FF column at 4 °C, and the SMG7 (Nde I) fragment was eluted with a buffer which does not contain glutathione.

Phage Biopannning

Peptide sequences were selected from a commercially available disulfide constrained 7-mer random library displayed on phage M13 via N-terminal fusion to the minor coat protein, g3p, with a diversity of 1.3×10^9 (Ph. D-C7C™ phage display peptide library kit, new England Biolabs, Beverly, MA, USA). After a third round of amplification for binding SMG7 (Nde I) protein, individual phage were isolated, and the peptide sequences they displayed were deduced after DNA sequencing.

Molecular Modeling, Docking Simulation

Three-dimensional structures of peptides and SMG7 were constructed with MOE (version 2006.0801, CCG Inc., Montreal, Canada) based on the Brookhaven Protein Databank 1YA0. Docking simulation and the calculation of interaction energy of peptide with SMG7 were performed with using Amber99 force field in MOE. The resulting three-dimensional structures of the complexes were displayed by MolFeat (Ver. 3.5, FiatLux, Tokyo, Japan).

Pull-Down Assay

Cysteine-constrained peptides with biotinylated amino termini were purchased from Scrum co. Ltd (Tokyo, Japan). Intramolecular disulfide bridge formation of the peptides was characterized by matrix-assisted laser desorption/ionization time-of-flight mass spectroscopy before and after reduction using dithiothreitol (1mM) and by their unreactivity to Ellman's reagent, a sulfhydryl assay reagent (Pierce, Rockford, IL, USA). Pull-down assay of GST-SMG7 fusion protein by biotinylated peptides was performed using μMACs Streptavidin kit (Miltenyi Biotech GmbH, Bergisch Gladach, Germany) according to the manufactures instructions. Briefly, GST-SMG7 (Nde I) was mixed with individual biotinylated peptides (100 pmol) in Buffer A (50 mM Tris-HCl 100 mM NaCl, 1 mM EDTA, 1mM Phenylmethylsulfonyl fluoride) at a final volume of 200 μl and incubated at 4 °C for 1 hour. Then, 100 μl of streptavidin magnetic beads were added and incubated at 4 °C for further 30 min. The reaction mixture was passed through a μ column (Miltenyi Biotech GmbH) and proteins bound to the biotinylated peptides were eluted using 70 μl of boiled sodium dodecyl sulfate-polyacrylamide gel electrophoresis (SDS-PAGE) loading buffer. As a negative control, GST protein was used in combination with the peptides. The eluted protein samples were analyzed by 10% SDS-PAGE.

RESULTS

Phage Display Screening of SMG7 Binding Peptides

To identify peptide ligands for the N-terminal and tetratricopeptide repeat (TPR)-containing domain of SMG7 protein, a disulfide bond-constrained random 7-mer peptide phage display library was screened with the amino terminal half of recombinant SMG7 protein, SMG7 (Nde I). During the course of selection, the relative yield of phage recovery improved from 0.0005% (first round) to 0.013% (third round), which is consistent with enrichment in binding clones. Forty clones after 3 rounds of panning were amplified and subjected to DNA sequence analysis to identify the displayed peptide. Four clones out of 40 contained truncated or duplicated peptide sequences. The remaining 36 clones yielded peptide sequences, however, there were no typical motifs or consensus sequences among them.

Evaluation of the Results of Phage Display by Docking Simulation and Pull Down Assay

We employed a docking simulation analysis to predict the rank orders of the binding affinities of the 36 peptide sequences with the TPR-containing domain of SMG7. First, we determined the possible peptide binding site in SMG7 (W61, K66, Q73, D160, R163, N190 and Q191) (Fig. **1**) by comparing the crystal structure of the N-terminal domain of SMG7 [14] to the ζ isoform of 14-3-3 in complex with a peptide ligand derived from phage display [17]. Next, we constructed the three dimensional structure of the 36 cyclic peptides by molecular modeling and simulation. Then, we performed the docking simulation of the 36 cyclic peptides with SMG7 and made the rank order of them according to their calculated docking energy (Fig. **2**). Fig. (**3**) shows the three-dimensional (3D) structures and the images for computational prediction of the interaction between SMG7 and each peptide for three candidate peptides (peptides 1, 4 and 19) that have the highest docking energies (-125.3, -149.6 and -116.8 kcal/mol, respectively) among 36 peptides.

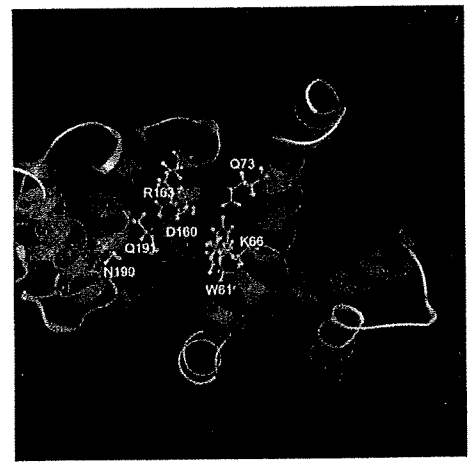

Figure 1. Structure of the N-terminal, TPR-containing domain, of human SMG7 protein. The ribbon diagram was generated as described in MATERIALS AND METHODS. Putative active amino acid residues, which may be responsible for interaction with peptides, are visually-enhanced.

To validate the result of docking simulation analysis, we investigated the relative affinity of the three candidate pep-

tides to SMG7 *in vitro* using a pull-down assay. We observed the difference in the binding affinities of the three peptides to recombinant SMG7 protein (Fig. **4**). Peptide 4, which has the highest rank by the docking simulation, showed the strongest binding to SMG7 of the three selected peptides. On the other hand, the three peptides did not bind to the control GST protein. These results suggest that docking simulation analysis can help in the selection of candidate peptides binding to a target protein when no consensus sequence is present in the peptides (obtained by phage display analysis).

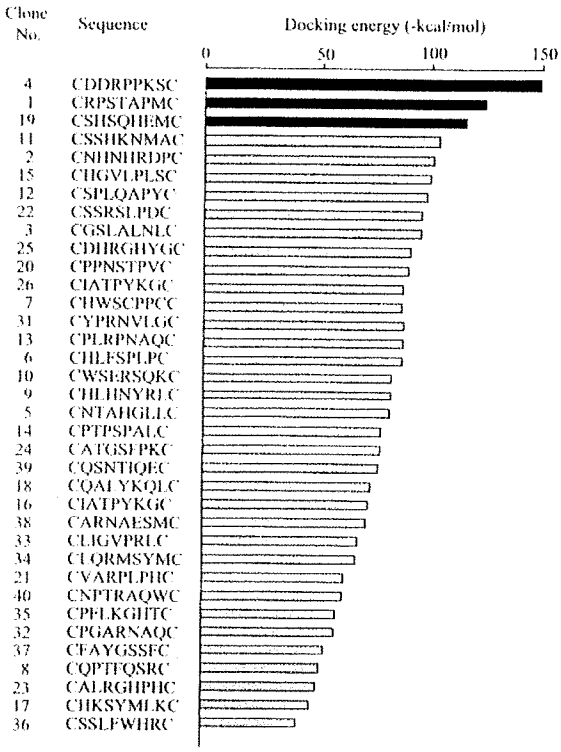

Figure 2. The docking energy of candidate peptides. Peptides were ranked with respect to their docking energy. Lower docking energy expects higher binding activity of the peptide to SMG7. Docking energy of the top 3 ranked peptides is accentuated in black.

DISCUSSION

Phage display technology is well known as a powerful tool for selecting peptides with desired biological and physiochemical properties from huge libraries. This technology has brought about major developments in peptide drug discovery. However, quite a few projects have produced a blind array due to the unexpected result that no consensus motif was found in the isolated clones (due to unknown and/or uncontrollable reasons). Our phage display screening of SMG7-binding peptides produced peptides with no consensus sequence. We could not align any of the 36 candidate peptide sequences with any consensus amino acid sequence. One of the strategies for breaking for the stalemate is to sequence of more candidates and determine the binding of each candidate to the target protein until a high affinity peptide candidate is obtained. However, this may be both time consuming and expensive.

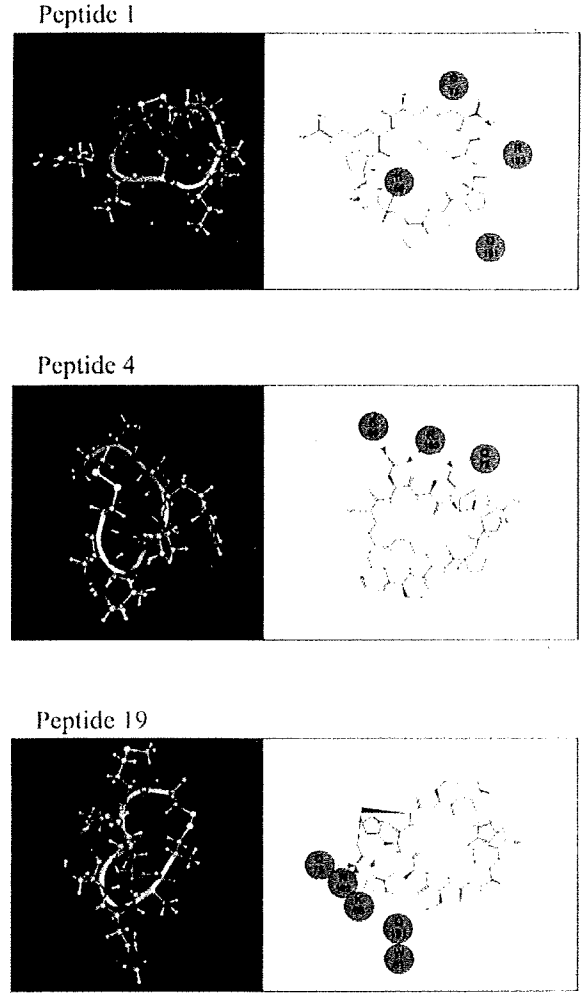

Figure 3. Structure of the top 3 ranked peptides (left) and schematic diagrams of the peptide-SMG7 binding (right).

On the other hand, an *in silico* screening technology (computational calculation for docking potential of small molecule ligands based on the binding pocket of protein receptors) has been developed and used for drug discovery [8, 9]. This docking simulation technology can be applied to find peptide ligands in addition to phage display. However, peptide docking simulation takes more time than docking simulation of small molecules because of the structural flexibility of peptides. It is difficult to evaluate the peptide library comprehensively by means of a docking simulation. To succeed in finding peptide ligands *in silico*, some ingenuity is needed to reduce the number of evaluated peptides, such as using the genetic algorithms [18, 19].

In this study, we applied the docking simulation analysis for our *in vitro* selected 36 peptides (Fig. **2**). We selected the top three-ranked peptides, made their 3D structure and docking image (Fig. **3**), allowing for the image of binding of the

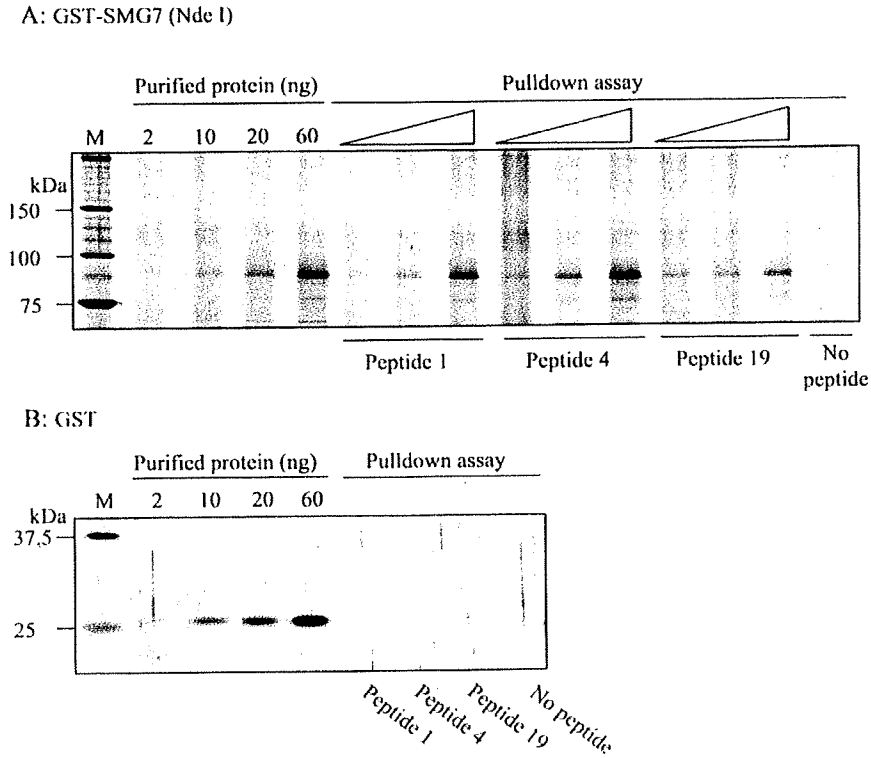

Figure 4. Binding of peptides 1, 4 and 19 to SMG7 *in vitro*. 100 pmol of each biotinylated peptide was incubated with 100, 300 and 1000 pmol of GST-SMG 7 (Nde I) recombinant protein (**A**) or 1000 pmol of GST protein (**B**). Protein bound to the peptide was collected in the streptavidin column and eluted with 70 µl of SDS sample buffer. A 10 µl aliquot of each sample was electrophoresed on SDS-polyacrylamide gel and visualized by silver staining. As a reference, 2 to 60 ng of the recombinant protein was also loaded in the same gel.

peptides into the TPR-containing pocket domain of SMG7. Finally, we examined their binding to SMG7 *in vitro* (Fig. **4**) and found that peptide 4 is an SMG7-binding peptide with a relatively high affinity. Therefore, this computational strategy allowed an early solution to the problem where a consensus motif cannot be found in the candidates screened by phage display.

In conclusion, these results suggest that docking simulation analysis in parallel with phage display is useful to determine the possible binding potential of peptides to the target protein rapidly and inexpensively. The docking simulation results are in good agreement with the result of binding affinity revealed by *in vitro* pull-down assay. Thus a combination of experimental and computational strategies enables us to retrieve positive peptide sequences successfully from the phage display-selected candidates, even if a consensus sequence cannot be found among the candidates.

ACKNOWLEDGEMENTS

This work was supported in part by Industrial Technology Research Grant Program '04 from the New Energy and Industrial Technology Development Organization (to T. S. and K. H.) and a 2007 Research Grant of Futaba Electronics Memorial Foundation (to Y. T).

ABBREVIATIONS

NMD	=	Nonsense-mediated mRNA decay
GST	=	Glutathione S-transferase
SDS-PAGE	=	Sodium dodecyl sulfate-polyacrylamide gel electrophoresis
TPR	=	Tetratricopeptide repeat

REFERENCES

[1] Smothers, J.F.; Henikoff, S.; Carter, P. Tech Sight. Phage display. Affinity selection from biological libraries. *Science*, **2002**, *298*, 621.

[2] Bair, C.L.; Oppenheim, A.; Trostel, A.; Prag, G.; Adhya, S. A phage display system designed to detect and study protein-protein interactions. *Mol. Microbiol.*, **2008**, *67*, 719.

[3] Lee, C.M.; Iorno, N.; Sierro, F.; Christ, D. Selection of human antibody fragments by phage display. *Nat. Protoc.*, **2007**, *2*, 3001.

[4] Ashfield, R.; Jakobsen, B.K. Making high-affinity T-cell receptors: a new class of targeted therapeutics. *IDrugs*, **2006**, *9*, 554.

[5] Mohammadi, M.; Rasaee, M.J.; Rajabibazl, M.; Paknejad, M.; Zare, M.; Mohammadzadeh, S. Epitope mapping of PR81 anti-MUC1 monoclonal antibody following PEPSCAN and phage display techniques. *Hybridoma (Larchmt)*, **2007**, *26*, 223.

[6] Wright, R.M.; Dudas, D.; Gavin, B.; Dottavio, D.; Hexham, J.M.; Lake, P. A high-capacity alkaline phosphatase reporter system for the rapid analysis of specificity and relative affinity of peptides from phage-display libraries. *J. Immunol. Methods*, **2001**, *253*, 223.

[7] Christian, R.B.; Zuckermann, R.N.; Kerr, J.M.; Wang, L.; Malcolm, B.A. Simplified methods for construction, assessment

and rapid screening of peptide libraries in bacteriophage. *J. Mol. Biol.*, **1992**, *227*, 711.

[8] McInnes, C. Virtual screening strategies in drug discovery. *Curr. Opin. Chem. Biol.*, **2007**, *11*, 494.

[9] Moitessier, N.; Englebienne, P.; Lee, D.; Lawandi, J.; Corbeil, C.R. Towards the development of universal, fast and highly accurate docking/scoring methods: a long way to go. *Br. J. Pharmacol.*, **2008**, *153* (Suppl 1), S7.

[10] Betzi, S.; Restouin, A.; Opi, S.; Arold, S.T.; Parrot, I.; Guerlesquin, F.; Morelli, X.; Collette, Y. Protein protein interaction inhibition (2P2I) combining high throughput and virtual screening: Application to the HIV-1 Nef protein. *Proc. Natl. Acad. Sci. USA*, **2007**, *104*, 19256.

[11] Harkcom, W.T.; Bevan, D.R. Molecular docking of inhibitors into monoamine oxidase B. *Biochem. Biophys. Res. Commun.*, **2007**, *360*, 401.

[12] Taylor, P.; Blackburn, E.; Sheng, Y.G.; Harding, S.; Hsin, K.Y.; Kan, D.; Shave, S. Walkinshaw, M.D. Ligand discovery and virtual screening using the program LIDAEUS. *Br. J. Pharmacol.*, **2008**, *153* (Suppl 1), S55.

[13] Unterholzner, L.; Izaurralde, E. SMG7 acts as a molecular link between mRNA surveillance and mRNA decay. *Mol. Cell*, **2004**, *16*, 587.

[14] Fukuhara, N.; Ebert, J.; Unterholzner, L.; Lindner, D.; Izaurralde, E.; Conti, E. SMG7 is a 14-3-3-like adaptor in the nonsense-mediated mRNA decay pathway. *Mol. Cell*, **2005**, *17*, 537.

[15] Wang, B.; Yang, H.; Liu, Y.C.; Jelinek, T.; Zhang, L.; Ruoslahti, E.; Fu, H. Isolation of high-affinity peptide antagonists of 14-3-3 proteins by phage display. *Biochemistry*, **1999**, *38*, 12499.

[16] Nagase, T.; Seki, N.; Ishikawa, K.; Ohira, M.; Kawarabayasi, Y.; Ohara, O.; Tanaka, A.;; Kotani, H.; Miyajima, N.; Nomura, N. Prediction of the coding sequences of unidentified human genes. VI The coding sequences of 80 new genes (KIAA0201-KIAA0280) deduced by analysis of cDNA clones from cell line KG-1 and brain. *DNA Res.*, **1996**, *3*, 321.

[17] Petosa, C.; Masters, S.C.; Bankston, L.A.; Pohl, J.; Wang, B.; Fu, H.; Liddington, R.C. 14-3-3ζ binds a phosphorylated Raf peptide and an unphosphorylated peptide via its conserved amphipathic groove. *J. Biol. Chem.*, **1998**, *273*, 16305.

[18] Abe, K.; Kobayashi, N.; Sode, K.; Ikebukuro, K. Peptide ligand screening of alpha-synuclein aggregation modulators by *in silico* panning. *BMC Bioinformatics*, **2007**, *8*, 451.

[19] Yagi, Y.; Terada, K.; Noma, T.; Ikebukuro, K. Sode, K. *In silico* panning for a non-competitive peptide inhibitor. *BMC Bioinform.*, **2007**, *8*, 11.

Received: May 20, 2008 **Revised: June 19, 2008** **Accepted: June 25, 2008**

Molecular Microbiology (2009) 74(1), 85–97 ■

doi:10.1111/j.1365-2958.2009.06852.x
First published online 2 September 2009

Replacement of the λ boxB RNA–N peptide with heterologous RNA–peptide interactions relaxes the strict spatial requirements for the formation of a transcription anti-termination complex

Satoru Horiya,[1] Mitsuru Inaba,[2] Chang-Song Koh,[2] Hiroaki Uehara,[2] Naomi Masui,[2] Misa Mizuguchi,[2] Masaya Ishibashi,[3] Senya Matsufuji[1] and Kazuo Harada[2]*

[1]*Department of Molecular Biology, The Jikei University School of Medicine, Minato-ku, Tokyo 105-8461, Japan.*
[2]*Department of Life Sciences, Tokyo Gakugei University, Koganei-shi, Tokyo 184-8501, Japan.*
[3]*Shinkasoyaku Corp., Yokohama-shi, Kanagawa 240-0064, Japan.*

Summary

In bacteriophage λ, formation of a transcriptional anti-termination complex involving the elongating RNA polymerase is mediated by the interaction of boxB RNA with the RNA-binding domain of the N protein (N peptide). In an attempt to understand the spatial requirements for boxB/N peptide interaction within the anti-termination complex, the effects of changes in the distance between boxA and boxB RNA, the length of the boxB stem, and the distance between the N peptide and remainder of the N protein were examined using a bacterial reporter system. It was found that the requirements for boxB stem length and the distance between N peptide and the remainder of N were optimized and strict. In contrast, replacement of the boxB/N interaction by heterologous RNA–peptide interactions appeared to relax the strict requirement for RNA stem length and the orientation of the RNA-binding peptide, presumably due to the absence of the cooperative interaction between boxB/N and the host factor NusA. In addition, the decrease in activity upon stem lengthening could be partially suppressed by simultaneous lengthening of the RNA spacer. A further understanding of the structural organization of the anti-termination complex may provide insights into how functional ribonucleoprotein complexes may be engineered.

Accepted 7 August, 2009. *For correspondence. E-mail harada@u-gakugei.ac.jp; Tel. (+81) 42 329 7550; Fax (+81) 42 329 7550.

Introduction

In bacteriophage λ, the expression of early operons is controlled by λ N protein through suppression of transcription termination at both Rho-dependent and intrinsic (Rho-independent) termination sites (Das, 1993; Greenblatt *et al.*, 1993; Nudler and Gottesman, 2002; Vieu and Rahmouni, 2004). *cis*-acting elements termed *nut* (N-utilization) sites (*nut*L and *nut*R) are situated between the promoters p_L and p_R and the first terminator of the early operons and are necessary for N-mediated anti-termination (Rosenberg *et al.*, 1978; Salstrom and Szybalski, 1978). The *nut* sites consist of three elements, boxA (Olson *et al.*, 1982; Mogridge *et al.*, 1998a), boxB, which codes for a hairpin RNA (Rosenberg *et al.*, 1978; Somasekhar *et al.*, 1982), and a short intervening spacer. Anti-termination occurs when the NH_2-terminal arginine-rich region of the N protein binds to the boxB hairpin within the *nut* site of the nascent transcript and promotes the assembly of an anti-termination complex (Lazinski *et al.*, 1989; Greenblatt *et al.*, 1993; Chattopadhyay *et al.*, 1995; Tan and Frankel, 1995; Van Gilst *et al.*, 1997). Many protein–protein and RNA–protein interactions are required for this complex to form (Greenblatt *et al.*, 1993). Typically, *Escherichia coli* host factors NusA, NusG, NusB and S10, and another *nut* RNA element, boxA, are needed for assembly (Mogridge *et al.*, 1995) (Fig. 1), although anti-termination has been shown to occur in the absence of some factors under certain conditions (Whalen *et al.*, 1988; Rees *et al.*, 1996; Gusarov and Nudler, 2001).

The interaction of the NH_2-terminal arginine-rich region of the λ N protein (the N peptide) with the boxB element has been characterized in considerable detail. The λ boxB RNA consists of 15 nucleotides (nts), and folds into a hairpin structure that contains a pentaloop which forms a structure resembling that of the GNRA-tetraloop (where N is G, A, U or C; R is G or A) upon binding to a bent α-helix

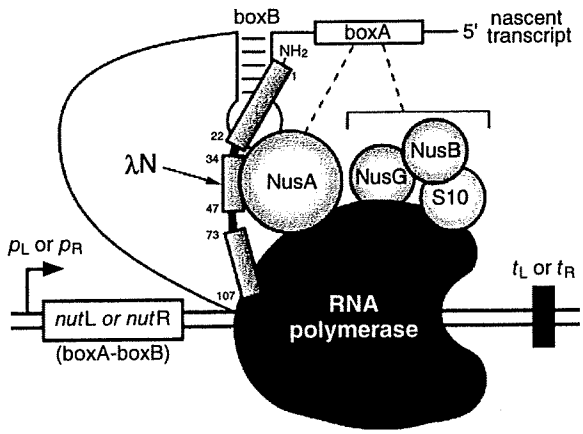

Fig. 1. λ anti-termination complex. Factors in contact and linked by broken lines have been shown to interact with each other by genetic and biochemical analysis (Mogridge *et al.*, 1995).

conformation of the N peptide (Tan and Frankel, 1995; Su *et al.*, 1997a,b; Legault *et al.*, 1998; Schärpf *et al.*, 2000). The boxB/N structure is well conserved among the lambdoid phages P22 (Tan and Frankel, 1995; Cai *et al.*, 1998) and phi21 (Cilley and Williamson, 2003), while showing somewhat different modes and specificities of binding (Austin *et al.*, 2003; Franklin, 2004). In the case of λ, N peptide-dependent folding of the boxB pentaloop into a GNRA-like structure results in the flipping out of the fourth nucleotide in the loop, and by doing so forms the NusA-binding site (Legault *et al.*, 1998).

A two-plasmid reporter system based on λ anti-termination that can be used to monitor the core interaction between the boxB RNA stem-loop and the N peptide has been developed by Franklin (1993). In this system, N is expressed from a pBR322-based plasmid, and β-galactosidase is expressed from a second pACYC-based reporter plasmid. The reporter plasmid contains four tandem repeats of the strong transcription terminator *t*1 from the *rrn*B operon, which are located downstream of the *nut* site and upstream of *lacZ*. When the N protein expressed from the first plasmid binds to the boxB hairpin expressed from the reporter plasmid, an anti-termination complex forms (Fig. 1), leading to anti-termination through the terminator sequences and expression of β-galactosidase. It has been shown that the boxB RNA hairpin and the NH_2-terminal boxB-binding domain of the N protein (residues 1–20) can be substituted by heterologous pairs of RNAs and polypeptides, thereby enabling the detection of interactions between arginine-rich peptides such as the human immunodeficiency virus (HIV) Rev peptide, a Zif268–Rev fusion, bovine immunodeficiency virus (BIV) Tat peptide, and proteins such as snRNP U1A protein and R17 coat protein, with their counterpart RNAs (Harada *et al.*, 1996; Wilhelm and Vale, 1996; McColl *et al.*, 1999; Peled-Zehavi *et al.*, 2003). Despite a decrease in anti-termination activity upon introduction of heterologous interactions, presumably due to the loss of the interaction between the NusA protein and the boxB/N complex, the two-plasmid system has been shown to be a sensitive method for the analysis of small changes in binding affinity of RNA–polypeptide interactions. This bacterial system has also been shown to be a powerful tool in the screening and selection of novel RNA-binding peptides targeting the HIV Rev-response element (RRE) from combinatorial libraries (Harada *et al.*, 1996; 1997; Peled-Zehavi *et al.*, 2003; Sugaya *et al.*, 2008a), as well as for the selection of novel peptide-binding RNAs (Iwazaki *et al.*, 2005; Sugaya *et al.*, 2008b). However, there appeared to be limitations on the size of RNAs that can be accommodated in the anti-termination complex, with only the interaction of relatively small RNA stem-loops with their cognate polypeptides being detected using the two-plasmid system. While the types of heterologous RNAs and peptides that can be introduced into the anti-termination complex have not been systematically examined, some variability in the distance between the boxA and boxB elements seems to be tolerated (Neely and Friedman, 1998; 2000).

In this study, in order to understand the spatial requirements within the anti-termination complex for detection of RNA–polypeptide interactions, and to gain insight into the structural organization of the anti-termination complex, we examined the effect of the spatial context of the boxB or other RNA sites with respect to the boxA element, and of the distance between the N-peptide (residue 1–20) or other RNA-binding peptides and the remainder of the N protein (residue 21–107). We utilized the two-plasmid assay described above (Franklin, 1993) and its modified systems in which the boxB RNA–N peptide interaction (boxB/N) was replaced with the heterologous RNA–protein complexes of the RRE RNA and the Rev peptide (RRE/Rev), the BIV *trans*-acting responsive element (TAR) RNA and the BIV Tat peptide (TAR/Tat), U1 hairpin II (hpII) RNA and the U1A protein (hpII/U1A), and the complexes of two selected RRE-binding peptides, RSG-1.2 and K1, with the RRE (RRE/RSG-1.2 and RRE/K1 respectively) (Harada *et al.*, 1996; 1997; Harada and Frankel, 1998; Peled-Zehavi *et al.*, 2003). The use of heterologous interactions was expected to be informative because the structures of the RNA–peptide complexes are diverse, and may be expected to impose different spatial requirements on the anti-termination complex. The Rev and K1 peptides bind to an internal loop of RRE IIB in α-helical conformations (Tan *et al.*, 1993; Battiste *et al.*, 1996; Sugaya *et al.*, 2008a), the RSG-1.2 peptide binds to the same site in an extended-turn-helix conformation (Gosser *et al.*, 2001; Zhang *et al.*, 2001), the BIV Tat peptide binds to the BIV TAR bulge in a β-hairpin conformation (Puglisi *et al.*, 1995), and the U1A

protein binds to the apical loop of the U1 hpII as an RNP motif (Oubridge *et al.*, 1994).

We found that lengthening the boxB stem and insertion of a peptide spacer between residues 20 and 21 of N dramatically reduced anti-termination activity, presumably due to the strict spatial requirements for the formation of the boxB/N/NusA ternary complex, while increasing the distance between the boxA and boxB elements led to only a gradual decrease in activity. In contrast, replacement of the boxB/N complex with the heterologous RNA–peptide interactions led to a considerable relaxation in the stringency of the length of the peptide linker in particular, and also stringency of the RNA stem length, although to a lesser extent. In addition, simultaneous lengthening of the *nut* spacers was shown to partially compensate for the loss of function by the stem elongation in some cases. These results suggest that a further understanding of the spatial requirements of the anti-termination complex may enable the incorporation of a wider range of RNA–polypeptide complexes in the place of the boxB–N peptide complex, thereby demonstrating how a functional ribonucleoprotein complex may be engineered in a predictable manner.

Results

Lengthening the stem of boxB and heterologous RNA sites

The effect of the insertion of RNA duplexes into the base of the boxB and U1 hpII stem, and the lower stem of the RRE and TAR stem-loop was examined (Fig. 2A and B, Table S1). *LacZ* reporter plasmids where 5 or 11 base pair (bp) duplexes were inserted into the base of the λ *nut*R boxB or a *nut* site in which boxB was replaced with HIV RRE, BIV TAR or U1 hpII (designated st+5 or st+11, Fig. 2A) were constructed. The secondary structures of the RNAs were consistent with those obtained using the MFOLD RNA folding algorithm (Jaeger *et al.*, 1989; 1990; Zuker, 1989) (data not shown). Anti-termination activities in the presence of the cognate or non-cognate binding peptide or protein were assayed for β-galactosidase activity by colony colour assays on plates containing 5-bromo-4-chloro-3-indolyl-β-D-galactopyranoside (Xgal), and in solution using o-nitrophenyl-β-D-galactopyranoside (ONPG). We have already shown that anti-termination activities reported using β-galactosidase and scored as the intensity of colony colour correlates well with the strength of the RNA–peptide interaction replacing the boxB RNA and N peptide, and should be an accurate measure for the stability of the anti-termination complex. Colony colour was scored from 0 to 8 plusses (8+) by comparison with a standardized set of controls (see Fig. 3 for representative colony colours). For example, the interaction between the RRE RNA and the DLA peptide (Kd = 0.5 nM), which is related to the K1 peptide used in this study, reported an anti-termination activity of 6+ (Sugaya *et al.*, 2008a), while that of the RRE and the RSG-1.2 peptide (Kd = 6 nM) was 5+ (Harada *et al.*, 1997), and that of the RRE and the Rev peptide (Kd = 40 nM) was 3+ (Harada *et al.*, 1996), where the number of plusses corresponds to the intensity of blue colony colour. One colony colour unit has been shown to correspond to roughly a fivefold difference in RNA–peptide binding affinity (M. Sugaya and K. Harada, unpublished data).

When 5 bp and 11 bp stems were inserted into the bottom of the boxB RNA stem-loop, a complete loss in anti-termination activity (scored as 0) from a colony colour of 8+ in the wild-type context (designated st+0) was observed (Fig. 2B). However, when the boxB/N interaction was replaced by the heterologous interactions, with the exception of RRE/RSG-1.2, residual activity of 0.5+ to 1.5+ was observed upon insertion of a 5 bp stem (st+5), showing that the lengthening of the stem was less disrupting with the heterologous RNA–polypeptide interactions. This difference in the effect of stem lengthening between the wild-type boxB/N and the heterologous interactions is presumably related to the presence of the boxB/N/NusA ternary complex in the wild-type context, which is absent in the case of the heterologous interactions.

In the case of the hpII/U1A, RRE/K1 and RRE/Rev interactions, further lengthening of the stem (st+11) did not reduce activity, and in the case of RRE/K1, a slight increase in activity from 1+ to 1.5+ (Fig. 2B), which was consistent with the results of the solution assay (Table S1), was observed. The copy number of the reporter plasmids was estimated by quantification of the amount of plasmid DNA per OD unit of bacterial culture, and were found to be similar (Fig. S1 and Table S2), showing that the differences in anti-termination activity were not due to changes in the amount of reporter plasmid. This suggested that the reduction in anti-termination activity was not simply the result of lengthening the RNA stem, but may also be due to the rotation of the RNA site around the helix axis. Indeed, lengthening of the upper stem region of the RRE had only a small effect on anti-termination activity (Fig. S2). Interestingly, when comparing the effect of the lengthening of the RRE stem in the presence of the K1 and Rev peptides, a somewhat similar behaviour was observed in that activity was retained for both st+5 and st+11, suggesting that the orientation of these two RNA–peptide complexes may be similar.

Intervening spacer between boxA and boxB

Next, the effect of the change in the length of the flexible single-stranded spacer connecting the boxA element and boxB or the heterologous RNA site on anti-termination activity was analysed. We constructed reporters that have

